Available online at www.sciencedirect.com
ScienceDirect
Journal of Luminescence 121 (2006) 456–464
JOURNAL OF LUMINESCENCE
www.elsevier.com/locate/jlumin

Time and temperature dependence of the emissions from the quantum-cutting phosphor $LiGdF_4$: Eu^{3+}

P. Vergeer*, E. van den Pol, A. Meijerink

Condensed Matter and Interfaces, Debye Institute, Utrecht University, P.O. Box 80000, 3508 TA Utrecht, The Netherlands

Received 7 September 2005; accepted 18 November 2005
Available online 28 February 2006

Abstract

The Gd–Eu couple is well known for efficient conversion of absorbed high-energy photons into two visible photons (quantum cutting). For this couple, a model describing the quantum-cutting mechanism has been proposed by Wegh et al. [J. Lumin. 82 (1999) 93]. This model is mainly supported by emission spectra, while the kinetics of the energy-transfer processes involved in quantum cutting have hardly been investigated. The present paper reports time and temperature dependent studies of the spectroscopic properties of $LiGdF_4$: Eu^{3+} 0.5%. The experimentally observed decay curves at room temperature of the Eu^{3+} $^5D_0$, $^5D_1$ and Gd^{3+} $^6P_{7/2}$ emission can be explained by a parameter model based on the kinetics of the mechanism. The temperature-dependent study shows a change in the energy-transfer kinetics that is consistent with the absence of quantum cutting at low temperatures ($T<50$ K).

PACS: 78.55.Hx; 78.47.+p

Keywords: Quantum cutting; Gd; Eu; Downconversion

1. Introduction

There is an increasing demand for efficient vacuum-ultraviolet (VUV, $\lambda<200$ nm) phosphors for application in plasma display panels and mercury-free fluorescent tubes based on a Xe discharge. The 90% quantum efficiency of the present generation of VUV phosphors leaves room for improvement. The short-wavelength excitation light of the Xe discharge has enough energy to obtain two visible photons for each VUV photon absorbed. This process is generally known as quantum cutting.

In 1974, Piper et al. [1] and Sommerdijk et al. [2] reported on the first quantum-cutting phosphor. In their materials the Pr^{3+} ion shows a cascade emission, converting VUV radiation into 405 and 480 nm photons with a visible quantum efficiency

*Corresponding author. Tel.: +31 30 2533545; fax: +31 30 2532403.
E-mail address: p.vergeer@phys.uu.nl (P. Vergeer).

0022-2313/$ - see front matter © 2005 Elsevier B.V. All rights reserved.
doi:10.1016/j.jlumin.2005.11.011

of 140%. The Pr^{3+} cascade emission is not used in lighting applications since 405 nm radiation has a too low color rendering index.

A more recent discovery is quantum cutting by downconversion. In this concept two ions are used to split the excitation energy. A well-known example is the Gd–Eu couple, for which efficient quantum cutting has been demonstrated in a number of fluoride lattices [3–7].

A model for the quantum-cutting mechanism has been proposed by Wegh et al. [9] (see Fig. 1). After excitation in the Gd^{3+} ^6G_J levels, partial energy transfer to Eu^{3+} by cross relaxation takes place: Gd^{3+} ^6G_J, Eu^{3+} $^7F_1 \rightarrow Gd^{3+}$ ^6P_J, Eu^{3+} $^5D_0$, denoted 1 in Fig. 1. This yields one photon from the Eu^{3+} $^5D_0 \rightarrow {}^7F_J$ transition. Note that the cross-relaxation step is thermally activated [9]. There is no spectral overlap between the Eu^{3+} $^7F_0 \rightarrow {}^5D_0$ transition and Gd^{3+} $^6G_{7/2} \rightarrow {}^6P_J$ transitions, which prevents cross relaxation at low temperatures. After the cross-relaxation step, the remaining energy on Gd^{3+} is transferred in a second energy-transfer step from Gd^{3+} ^6P_J to Eu^{3+}, denoted 2 in Fig. 1, which yields the second photon from a Eu^{3+} $^5D_J \rightarrow {}^7F_J$ transition. The process denoted *C* in Fig. 1 stands for single-step energy transfer from Gd^{3+} ^6G_J to Eu^{3+}. After this energy-transfer step relaxation to the Eu^{3+} ^5D_J levels takes place and only one photon is emitted for each VUV photon absorbed. This process competes with cross relaxation and the ratio of the two processes determines the intrinsic quantum efficiency.

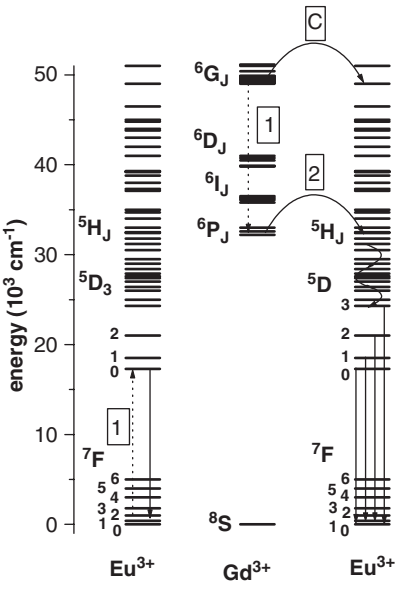

Fig. 1. Energy-level diagram for the Gd^{3+}–Eu^{3+} system, showing the possibility for cross relaxation (denoted by 1): $Gd^{3+}(^6G_J)$, Eu^{3+} $(^7F_1) \rightarrow Gd^{3+}(^6P_J)$, Eu^{3+} $(^5D_0)$. Subsequent energy transfer (denoted by 2) occurs from $Gd^{3+}(^6P_J)$ to Eu^{3+} (^5H_J). Energy transfer from $Gd^{3+}(^6G_J)$ to a high-energy level of Eu^{3+} is denoted by *C*.

In previous studies, quantum cutting has been demonstrated by studying emission and excitation spectra. In case of quantum cutting, an increase in the intensity of the Eu^{3+} $^5D_0 \rightarrow {}^7F_J$ emission to the $^5D_1 \rightarrow {}^7F_J$ emission is observed upon excitation in the Gd^{3+} ^6G_J levels [3–7].

The analysis of the emission spectra gives insight in the quantum-cutting process via time-integrated luminescence and no information is obtained on the kinetics of the energy-transfer processes involved. After Gd^{3+} ^6G_J excitation, a relatively fast increase in the time-resolved signal of the Eu^{3+} $^5D_0$ emission is expected as compared to the increase in the $^5D_1$ emission intensity, since the $^5D_0$ level is populated directly in the cross-relaxation step. Kondo and coworkers have done time-dependent luminescence studies on the Eu^{3+} $^5D_{1,0} \rightarrow {}^7F_J$ emission in $NaGdF_4$: Eu^{3+} and have observed this [5]. However, upon excitation into the ^6I_J levels of Gd^{3+} the Eu^{3+} ^5D_J emissions show a strong instant signal which is in contradiction with the kinetics of the quantum-cutting model.

In this work the dynamics of the Gd^{3+} ^6P_J, Eu^{3+} $^5D_1$ and the Eu^{3+} $^5D_0$ emissions are investigated for $LiGdF_4$: Eu^{3+}. A parameter model based on the mechanisms described in Fig. 1 is used to fit to room-temperature (RT) decay curves of the Eu^{3+} emissions. A good agreement would provide further proof for the downconversion mechanisms as proposed in the quantum-cutting model and provide information on the kinetics of the steps involved. Also, temperature dependent spectra and decay curves are measured for the Gd^{3+} ^6G_J, ^6P_J, and the Eu^{3+} $^5D_1$ and $^5D_0$ emissions. Cross relaxation is expected to be absent at low temperatures (<50 K [9]) and thus a change in the luminescence decay properties is expected as a function of temperature.

2. Experimental

A powder sample was prepared by firing stoichiometric mixtures of LiF, GdF_3 and 0.5% EuF_3 at 550 °C in a nitrogen atmosphere. The sample was checked by X-ray diffraction and found to be single phase. $LiGdF_4$ is isostructural to $LiYF_4$, which has the inverse scheelite structure, space group $I4_{1/a}$.

For emission spectra at RT a SPEX DM-3000F spectrofluorometer adapted for the VUV was used [8]. The excitation source is a D_2-lamp (Hamamatsu L1835, 150 W). The excitation and emission light are both dispersed by double 0.22 m gratings (SPEX 1680, 1200 l/mm) blazed at 150 nm for the excitation light and at 500 nm for the emission light.

Decay curves at RT were measured with the use of two excitation sources. For excitation in Gd^{3+} ^6P_J levels a Lambda Physik LPD3000 tunable dye laser filled with a Rhodamine B dye solution was used. Radiation with a wavelength of 311.4 nm was created by second-harmonic generation of the dye-laser output with a KDP crystal. The dye laser was pumped by a Lambda Physik LPX100 excimer (XeCl) laser. For excitation in the Gd^{3+} ^6G_J levels a fluoride excimer laser (ExciStar S-200, Tuilaser) filled with an argon/fluorine gas mixture was used. The excitation wavelength is 193 nm and the pulse duration is typically 10 ns. Emission light was dispersed by an Acton Research monochromator (Scientific SpectraPro, 150 l/mm grating, blazed at 500 nm with 0.300 m focal length) and detected by a RCA C31034 photo multiplier tube (PMT). The signal from the PMT was amplified by an operational amplifier (10^4, response ~2 μs) and then registered with a Tektronix 2440 digital oscilloscope.

Temperature-dependent emission spectra and decay curves were measured with the fluoride excimer laser as excitation source (argon/fluorine gas mixture, 193 nm). The emission from the sample was dispersed by a 1200 l/mm grating (Jobin Yvon, Triax 550, blazed at 450 nm) and detected with a Hamamatsu R928 PMT. The signal from the PMT was amplified by an operational amplifier (10^4, response ~2 μs) and then registered with a Tektronix 2440 digital oscilloscope. Control over the temperature from 30 K to RT was achieved by mounting the sample on an Oxford Instruments Optistat$^{CF\text{-}V}$ liquid-helium cold-finger cryostat connected to an Oxford Intelligent Temperature Controller (ITC4). The temperature sensor of the temperature controller is mounted at the end of the cold finger and the measured temperature deviates from the actual temperature of the sample. The temperature of the sample was determined by comparing the Boltzman populations from the Stark levels of the Gd^{3+} $^6P_{7/2} \rightarrow {}^8S_{7/2}$ transition. For this purpose, high-resolution emission spectra were obtained in the wavelength region of 310.6–311.6 nm, with the use of a 3600 l/mm grating (Jobin Yvon, Triax 550) blazed for the VUV/UV.

3. Results and discussion

3.1. Spectroscopy and kinetics of quantum cutting at room temperature

Evidence for quantum cutting in Gd–Eu couples is commonly obtained by comparison of emission spectra at different excitation wavelengths. When excitation is into the Gd^{3+} ^6P_J, ^6I_J, or ^6D_J levels, a single energy-transfer step to Eu^{3+} occurs and the 'normal' branching ratio for the Eu^{3+} ^5D_J emission is obtained. This branching ratio is also observed after excitation of a high-energy Eu^{3+} energy level. It is determined by multi-phonon relaxation from the $^5D_3$ level to the lower-energy ^5D_J levels and, depending on the Eu^{3+} concentration, by cross relaxation between Eu^{3+} ions. An emission spectrum upon excitation in Gd^{3+} ^6P_J is plotted in Fig. 2a. The plot shows the Eu^{3+} $^5D_1$ and $^5D_0$ emissions. The same peaks were observed in previous work and they are assigned accordingly [9]. The spectrum is normalized to the Eu^{3+} $^5D_0 \rightarrow {}^7F_2$ emission peak. Fig. 2b shows the same emissions, but after excitation in Gd^{3+} ^6G_J. In order to show the effect of quantum cutting, the spectrum is scaled to the Eu^{3+} $^5D_1$ emission in Fig. 2a. The Eu^{3+} $^5D_0$ emissions have increased in intensity upon excitation in Gd^{3+} ^6G_J. The higher relative intensity of the $^5D_0$ emission lines in this scaled spectrum is the effect of the cross-relaxation

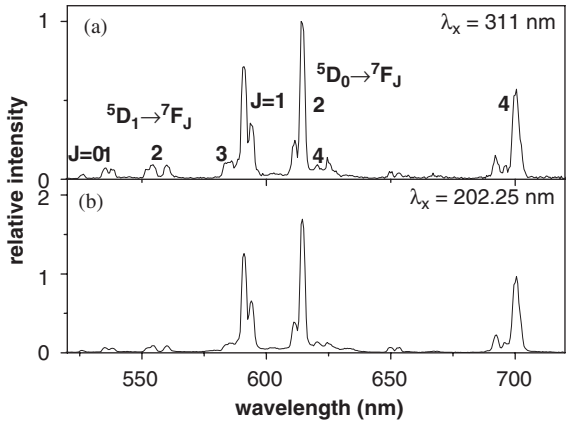

Fig. 2. Emission spectra (RT) of the Eu^{3+} $^5D_{1,0}$ emissions upon excitation into the Gd^{3+} ^6P_J levels (a) and into the Gd^{3+} ^6G_J levels (b).

step in Fig. 1. In this step only the Eu^{3+} $^5D_0$ level is populated, which leads to an increase of the $^5D_0$ emission after Gd^{3+} ^6G_J excitation.

The cross-relaxation efficiency can also be calculated from the emission spectra shown in Fig. 2 according to the equation proposed by Wegh et al. [9],

$$\frac{p_1}{p_1+p_C}=\frac{R(^5D_0/^5D_{1,2,3})_{^6G_J}-R(^5D_0/^5D_{1,2,3})_{^6P_J}}{R(^5D_0/^5D_{1,2,3})_{^6P_J}+1}. \quad (1)$$

Here, p_1 and p_C are the probabilities for cross relaxation and direct energy transfer from Gd^{3+} ^6G_J to Eu^{3+}, and $R(^5D_0/^5D_{1,2,3})_{^6G_J}$ and $R(^5D_0/^5D_{1,2,3})_{^6P_J}$ are the $^5D_0/^5D_{1,2,3}$ emission intensity ratios upon ^6G_J excitation and upon ^6P_J excitation. Evaluation of Eq. (1) gives a cross-relaxation probability of 58%. This means that the quantum efficiency is 158%. This value is lower than the value of 190% reported by Wegh et al. [9]. The lower efficiency of this sample is probably caused by defects in the sample. A defect emission is observed at low temperatures (see below).

Time-dependent measurements, with fits included, are shown in Fig. 3. In Fig. 3a the time-dependent traces are shown for the Eu^{3+} $^5D_1$ emission upon excitation in Gd^{3+} ^6P_J (triangles) and in Gd^{3+} ^6G_J (squares). Fig. 3b shows the time-dependent traces for the Eu^{3+} $^5D_0$ emission upon excitation in Gd^{3+}

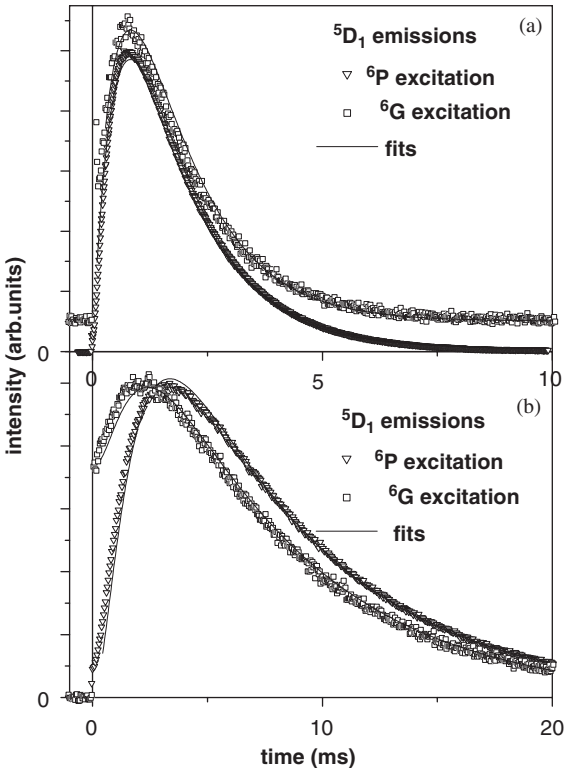

Fig. 3. (a) Time-resolved intensity of the $^5D_1$ emission (RT, 552 nm) for excitation into Gd^{3+} ^6P_J (311 nm, triangles) or into Gd^{3+} ^6G_J (193 nm, squares). The decay curve after ^6G excitation is shifted along the y-axis. (b) Time-resolved intensity of the $^5D_0$ emission (RT, 700 nm) for excitation into Gd^{3+} ^6P_J (311 nm, triangles) or into Gd^{3+} ^6G_J (193 nm, squares). Note the different time scales. Solid lines are fits to the experimental curves (see text).

^6P_J (triangles) and in Gd^{3+} ^6G_J (squares). The shape of the curves can be understood from the kinetics of the downconversion model described in Fig. 1 when a fast migration regime is assumed [10]. In the fast migration regime, the inter-Gd energy transfer is much faster than Gd–Eu energy transfer. Energy migration over Gd^{3+} ^6P_J levels in $LiGdF_4$ has been investigated and found to be a fast process ($10^{7\pm1}$ s^{-1} per Gd–Gd energy-transfer step) [11,12]. In this case, the inter-Gd energy migration, subsequent Gd–Eu energy transfer and fast multi-phonon relaxation on the Eu^{3+} ion can be described by one effective energy-transfer rate from Gd^{3+} $^6P_{7/2}$ to Eu^{3+} $^5D_1$. With this assumption, the following set of coupled differential rate equations is used to describe

relaxation after Gd^{3+} ^6P_J excitation:

$$\frac{dn_1}{dt} = \gamma_P n_P - \gamma_1 n_1,$$
$$\frac{dn_0}{dt} = \gamma_1 n_1 - \gamma_0 n_0. \quad (2)$$

In Eq. (2) n_1 stands for the population of Eu^{3+} ions in the $^5D_1$ excited state, n_P stands for the population of Gd^{3+} ions in the ^6P_J excited state and n_0 stands for the population of Eu^{3+} ions in the $^5D_0$ excited state. The effective rate constant for relaxation from Gd^{3+} ^6P_J to Eu^{3+} $^5D_1$ is denoted by γ_P, the rate constant for (radiative and non-radiative) decay from the Eu^{3+} $^5D_1$ level is given by γ_1 and the rate constant for radiative decay from the Eu^{3+} $^5D_0$ level by γ_0. In Eq. (2) the time dependence of the $^5D_1$ emission is described by a feeding and decaying term, with feeding from the Gd^{3+} ^6P_J levels. The resulting curve accurately describes the experimental curve in Fig. 3a. The values for γ_P ($1783\,s^{-1}$) and γ_1($778\,s^{-1}$) obtained from this fit were fixed at these values when subsequent rate equations were used for fitting. The time dependence of the population of the Eu^{3+} $^5D_0$ level is coupled to the time dependence of the population of the Eu^{3+} $^5D_1$ level since in Eq. (2) the $^5D_0$ level is fed by the $^5D_1$ level. The fit shows good agreement with the shape of the experimental curve in Fig. 3b when γ_0 is equal to $148\,s^{-1}$.

Relaxation after Gd^{3+} ^6G_J excitation is described by a similar set of coupled differential rate equations,

$$\frac{dn_P}{dt} = \gamma_G n_G - \gamma_P n_P,$$
$$\frac{dn_1}{dt} = \gamma_P n_P - \gamma_1 n_1,$$
$$\frac{dn_0}{dt} = \gamma_G n_G + \gamma_1 n_1 - \gamma_0 n_0, \quad (3)$$

where γ_G denotes the effective cross-relaxation rate that feeds both the $^5D_0$ level of Eu^{3+} and the ^6P levels of Gd^{3+}. When the two sets of coupled differential rate equations (Eqs. (2) and (3)) are compared, it is noted that upon Gd^{3+} ^6G_J excitation one equation is added, which describes the time dependence of the population of the Gd^{3+} ^6P_J levels. This is due to the fact that the Gd^{3+} ^6P_J levels are now fed by Gd^{3+} ^6G_J levels in the cross-relaxation step. In the experiment (Fig. 3a) the measured decay curve for the Eu^{3+} $^5D_1$ emission after Gd^{3+} ^6G_J excitation is almost identical to the one obtained after Gd^{3+} ^6P_J excitation. This shows that cross relaxation is a much faster process than energy transfer from Gd^{3+} ^6P_J to Eu^{3+} $^5D_1$ (otherwise the feeding of the $^5D_1$ emission would be slower due to the cross-relaxation step which feeds the ^6P level). This is to be expected since the effective rate constant for the Gd^{3+} $^6P_J \rightarrow Eu^{3+}$ energy transfer includes the relatively slow non-radiative relaxation processes to the $^5D_1$ level on the Eu^{3+} ion.

As a consequence of the fast cross-relaxation step, when monitoring the decay of the Eu^{3+} $^5D_0$ emission upon Gd^{3+} ^6G_J excitation an instant signal is expected due to fast feeding of the $^5D_0$ level through cross relaxation. This is exactly what is observed in the experimental results shown in Fig. 3b. The fit to the Eu^{3+} $^5D_0$ emission curve is done with all transition rates obtained from fits to the previous curves. The theoretical curve predicts the rise-time and the appearance of the instantaneous signal accurately. This gives a good indication that the model used is appropriate. Also, the theoretical curve reproduces the ratio between the instant signal and the rising signal in the experiment remarkably well. However, the good agreement on this point is somewhat fortuitous since the model contains two simplifications which influences seem to cancel each other. In the model, it is assumed that the cross-relaxation efficiency is 100%, leading to an increased contribution of the instantaneous signal as compared to the experiments. However, the model also assumes no radiative and non-radiative losses for the build-up component of the $^5D_0$ emission, leading to an increased contribution of the rising signal as compared to the experiment. Apparently, these two effects cancel each other.

The decay rates obtained are listed in Table 1. The value of $1783\,s^{-1}$ for γ_P mainly reflects the non-radiative relaxation processes on the Eu^{3+} ion. The (non-radiative) energy-transfer rate from the Gd^{3+} ^6P_J levels is found to be much faster: $1.7 \times 10^4\,s^{-1}$ (see below). The radiative decay rate for the Eu^{3+} $^5D_0$ emission is slow for a $4f^n \rightarrow 4f^n$

Table 1
Parameter values obtained for the rate constants in Eqs. (2) and (3) from fits to the luminescence decay curves in Fig. 3

	From	To	γ (s^{-1})
γ_P	Gd^{3+} ^6P_J	Eu^{3+} $^5D_1$	1783 (30)
γ_G	Gd^{3+} ^6G_J	Gd^{3+} ^6P_J	$>5\times10^4$
γ_1	Eu^{3+} $^5D_1$	–	778 (10)
γ_0	Eu^{3+} $^5D_0$	–	148 (2)

The numbers between brackets give the statistical 95% confidence interval. The solid lines in Fig. 3 show the decay curves obtained based on the parameter values.

transition. It corresponds to a lifetime of 6.7 ms, which is in agreement with the lifetime obtained after direct excitation into the $^5D_0$ level and slightly lower than the 7.3 ms obtained by others [13]. The confidence margins are 95% statistical confidence margins based on the fitting process. They give an indication of the quality of the fits. It is known that differences in the detection methods limit the accuracy of obtained decay rates to some 10%. The same detection equipment was used to obtain the four decay curves discussed above.

3.2. Temperature dependence

Apart from the kinetics, also the temperature dependence of the Gd–Eu quantum-cutting system is worth studying. Due to a mismatch in energy, energy transfer by cross relaxation is expected to be inefficient at low temperatures and changes in the visible spectra as a function of temperature have been observed [9]. The $^7F_0\rightarrow{}^5D_0$ energy difference is slightly ($\sim$250 cm^{-1}) larger than the $^6G_{7/2}\rightarrow{}^6P_{7/2}$ energy difference and phonon-assisted energy transfer or thermal population of the Eu^{3+} $^7F_1$ state or the higher crystal-field levels of the Gd^{3+} $^6G_{7/2}$ state is needed to overcome the mismatch. In Fig. 4 emission spectra are shown from 200 to 620 nm at various temperatures. All graphs are scaled on the Eu^{3+} $^5D_0\rightarrow{}^7F_1$ emission at 590.5 nm. At low temperatures, a defect band emission is observed in the blue spectral region. The presence of defects reduces the quantum efficiency of this phosphor.

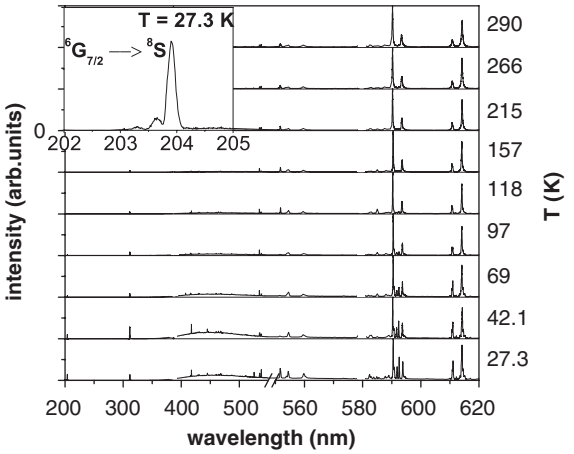

Fig. 4. Emission spectra of $LiGdF_4:Eu^{3+}$ 0.5% at various temperatures ($\lambda_x = 193$ nm). The reflection of the laser radiation in second (around 386 nm) and third (around 579 nm) order were removed from the spectra. Note the change in wavelength scale. The inset shows the Gd^{3+} $^6G_{7/2}\rightarrow{}^8S_{7/2}$ emission at 27.3 K.

In the red spectral region, Eu^{3+} emission lines are observed at all temperatures and the four dominant peaks at RT are assigned to Eu^{3+} $^5D_0$ emissions. When the temperature is decreased below 100 K more peaks around 592 nm start to appear. These are assigned to Gd^{3+} $^6G_J\rightarrow{}^6P_J$ emission lines [9]. They are most apparent at the lowest temperatures. The presence of the Gd^{3+} $^6G_{7/2}$ emission can be explained by less efficient cross relaxation. The thermally activated cross-relaxation process is inhibited at low temperatures. At temperatures higher than 100 K the $^7F_1$ level of Eu^{3+} and the Stark levels of the $^6G_{7/2}$ level of Gd^{3+} become sufficiently thermally populated to allow for efficient cross relaxation.

Furthermore, at short wavelengths ($\sim$204 nm), Gd^{3+} $^6G_{7/2}\rightarrow{}^8S_{7/2}$ emissions are observed at low temperatures. The inset shows the Gd^{3+} $^6G_{7/2}\rightarrow{}^8S_{7/2}$ emission spectrum at 27.3 K. Three peaks are observed at 203.30, 203.64 and 203.90 nm, corresponding to emissions from the different $^6G_{7/2}$ stark levels. The positions are consistent with the energies calculated and observed for the $^6G_{7/2}$ crystal-field levels from excitation spectra [8].

While the relative intensity of the Gd^{3+} ^6G_J emissions show a strong decrease with increasing temperature, the intensity of the Gd^{3+} ^6P_J

emission (311 nm) rises when the temperature is increased between 25 and 50 K and then decreases monotonously when the temperature is increased further. The rise is explained by increased feeding from the Gd^{3+} ^6G_J levels by the thermally activated cross-relaxation process, while energy migration over the $^6P_{7/2}$ levels leading to Gd^{3+} ($^6P_{7/2}$) $\rightarrow$ Eu^{3+} energy transfer is still inefficient. When the temperature is increased further, both energy-transfer steps become more efficient, leading to a decrease in ^6G_J and ^6P_J emission intensity and fast energy transfer to Eu^{3+}.

Overall, the temperature dependent emission spectra are in agreement with quantum cutting by a temperature-activated cross-relaxation process. Cross relaxation becomes efficient when the temperature is raised above 100 K. At lower temperatures Gd^{3+} $^6G_{7/2}$ emission is observed.

Next, temperature-dependent luminescence decay curves will be discussed in a qualitative manner. The increased influence of competing processes and the slowed-down energy migration at low temperatures inhibits a quantitative analysis due to the relatively large extension in parameters needed to describe the additional processes.

Temperature dependent decay curves of the Gd^{3+} ^6P_J emission are shown in Fig. 5. The oscillations at short times are due to instrumental response to a fast signal.

The luminescence decay curves reflect the qualitative discussion on the temperature dependence of the ^6P_J emission intensity. At the lowest temperature, the ^6P_J emission shows a decaying signal with a lifetime of 260 μs with a small feeding term. This lifetime is much faster than the radiative lifetime of 8.7 ms [11], which shows that migration and energy transfer is already present. When the temperature is raised to 42.1 K the feeding component becomes remarkably more pronounced in the decay curve. This component is attributed to cross relaxation from the Gd^{3+} $^6G_{7/2}$ level, which is in agreement with the observations in the emissions spectra. When the temperature is increased further, a feeding component is still apparent up to 157 K while the time to reach the maximum of the decay curve shifts to shorter times. This reflects an increase in the cross-relaxation rate from the Gd^{3+} $^6G_{7/2}$ level and the energy transfer rate from the $^6P_{7/2}$ level. For higher temperatures, a single-exponential decay function is measured. The observations are explained by more efficient feeding through cross relaxation and more efficient energy migration over the Gd^{3+} ^6P_J levels as the temperature is increased, which agrees with the quantum-cutting model. The RT lifetime of the ^6P_J emission is 60 μs.

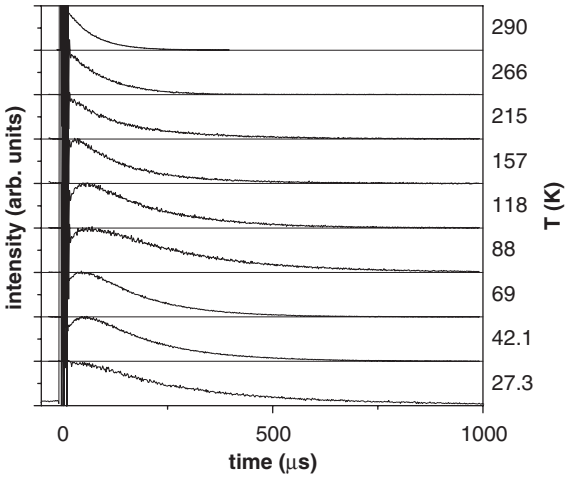

Fig. 5. Decay curves at various temperatures of the Gd^{3+} ^6P_J emission ($\lambda_x = 193$ nm, $\lambda_m = 311$ nm).

The temperature-dependent decay curves for the Eu^{3+} $^5D_1$ emission are shown in Fig. 6. The large signal at short time intervals is due to instrumental response.

At RT, a feeding process is observed in the decay curve, which is explained by non-radiative relaxation from the higher-energy ^5D_J levels. When the temperature is lowered to 100 K, relaxation rates slow down, which is indicated by an increase in the rise-time of the signals. When the temperature is lowered further, a large instant intensity and a relatively small feeding term are observed. Since the cross-relaxation probability is reduced at these low temperatures the origin of the large instant signal is attributed to competing processes such as energy transfer via the defect center. When the temperature is increased, quantum cutting becomes more probable and the feeding component becomes more pronounced.

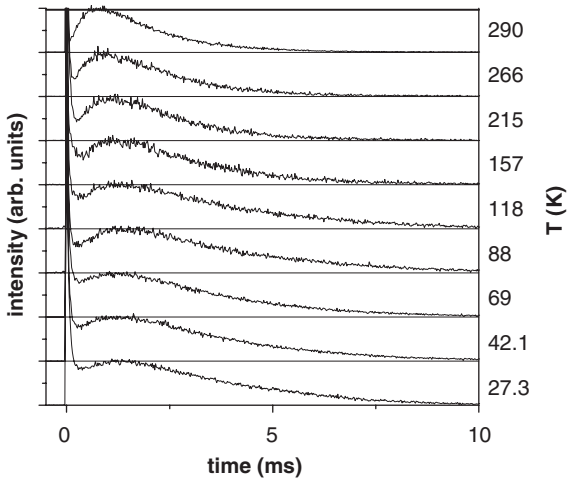

Fig. 6. Decay curves at various temperatures of the Eu^{3+} $^5D_1$ emission ($\lambda_x = 193\,nm, \lambda_m = 552\,nm$).

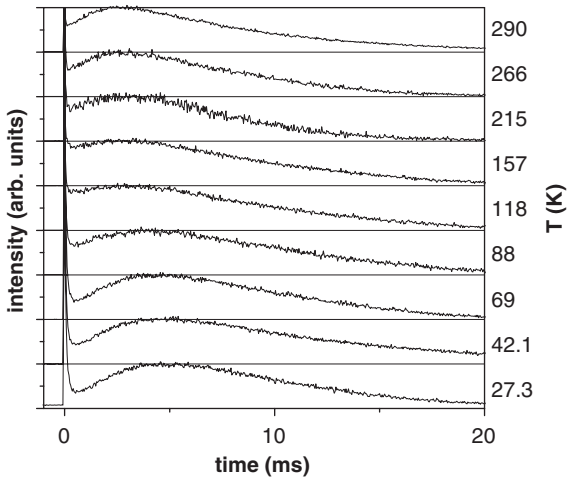

Fig. 7. Decay curves at various temperatures of the Eu^{3+} $^5D_0$ emission ($\lambda_x = 193\,nm, \lambda_m = 590.5\,nm$).

Fig. 7 shows the decay curves of the Eu^{3+} $^5D_0$ emission at several temperatures. The signal at short times is due to instrumental response.

All curves show a feeding component of which the rise-time increases when the temperature is lowered. Also, notable changes can be observed in the instantaneous signal of the decay curves as compared to the rise-time signal. From the low-temperature regime, the instantaneous signal is observed to increase when the temperature is increased to 157 K. Then, the feeding term becomes more apparent. The increase in the instantaneous signal can be explained by the enhancement of cross relaxation, which leads to a fast population of the Eu^{3+} $^5D_0$ level. When the temperature is increased further, the feeding term (caused by energy transfer from Gd^{3+} ^6P_J levels to Eu^{3+}) becomes more dominant, resulting in a relative decrease of the instant luminescence signal at temperatures above 157 K. At temperatures lower than 157 K the Eu^{3+} luminescence resulting from Gd^{3+} $^6P_J \rightarrow Eu^{3+}$ energy transfer is less dominant due to slower energy transfer and multi-phonon relaxation rates.

The decay curves of the Eu^{3+} $^5D_0$ level at various temperatures are in accordance with the decay curves from the Eu^{3+} $^5D_1$ level and the Gd^{3+} ^6P_J levels. They show a strong inhibition of cross relaxation and Gd^{3+} $^6P_{7/2} \rightarrow Eu^{3+}$ energy transfer at low temperatures. Cross relaxation becomes efficient when the temperature reaches 100 K, which agrees with the quantum-cutting model.

4. Conclusion

In this study the kinetics of the Gd–Eu down-conversion process were investigated by measuring emission spectra and time-dependent luminescence intensities for the Eu^{3+} $^5D_{1,0}$ and Gd^{3+} ^6G_J and ^6P_J emissions upon Gd^{3+} ^6P_J and ^6G_J excitation. Analysis of the RT luminescence decay curves shows that the experimental results can be explained by rate equations based on the down-conversion model. A good agreement is obtained between the various decay curves and fitted curves based on parameters for decay rates and energy-transfer rates for the various levels involved. Emission spectra and decay curves were measured as a function of temperature and showed that the cross-relaxation step is temperature activated and becomes efficient at temperatures above 100 K. The present analysis provides more insight in the kinetics of energy transfer processes in the Gd–Eu quantum-cutting system and the temperature dependence of the energy-transfer processes.

Acknowledgements

This research was supported by the Technology Foundation STW, applied science division of NWO and the technology programme of the Ministry of Economic Affairs.

References

[1] W.W. Piper, J.A. DeLuca, F.S. Ham, J. Lumin. 8 (1974) 344.
[2] J.L. Sommerdijk, A. Bril, A.W. De Jager, J. Lumin. 8 (1974) 341.
[3] R.T. Wegh, H. Donker, K.D. Oskam, A. Meijerink, Science 283 (1999) 663.
[4] B. Liu, et al., J. Lumin. 101 (2003) 155.
[5] H. Kondo, T. Hirai, S. Hashimoto, J. Lumin. 108 (2004) 59.
[6] N. Kodama, Y. Watanabe, Appl. Phys. Lett. 84 (2004) 4141.
[7] F. You, S. Huang, S. Liu, Y. Tao, J. Lumin. 110 (2004) 95.
[8] R.T. Wegh, et al., Phys. Rev. B 56 (1997) 13841.
[9] R.T. Wegh, H. Donker, K.D. Oskam, A. Meijerink, J. Lumin. 82 (1999) 93.
[10] B. Henderson, G.F. Imbusch, Optical Spectroscopy of Inorganic Solids, Clarendon Press, Oxford, 1989.
[11] H.S. Kiliaan, A. Meijerink, G. Blasse, J. Lumin. 35 (1986) 155.
[12] A.J. De Vries, M.F. Hazenkamp, G. Blasse, J. Lumin. 42 (1988) 275.
[13] J. van Vliet, D. van der Voort, G. Blasse, J. Lumin. 42 (1989) 305.